NuRD independent Mi-2 activity represses ectopic gene expression during neuronal maturation.

Gabriel N Aughey‡, Elhana Forsberg†, Krista Grimes†, Shen Zhang†, Tony D Southall*

†Equal contribution

*Correspondence to t.southall@imperial.ac.uk

Department of Life Sciences, Imperial College London, Sir Ernst Chain Building, London, UK

‡Current address: Department of Clinical and Experimental Epilepsy, UCL Queen Square Institute of Neurology, London, United Kingdom.

Abstract

During neuronal development, extensive changes to chromatin states occur to regulate lineage-specific gene expression. The molecular factors underlying the repression of non-neuronal genes in differentiated neurons are poorly characterised. The Mi2/NuRD complex is a multiprotein complex with nucleosome remodelling and histone deacetylase activity. Whilst NuRD has previously been implicated in the development of nervous system tissues the precise nature of the gene expression programmes that it coordinates are ill-defined. Furthermore, evidence from several species suggests that Mi-2 may be incorporated into multiple complexes that may not possess histone deacetylase activity. Here, we show that Mi-2 activity is required for suppressing the ectopic expression of germline genes in neurons independently of HDAC1/NuRD, whilst components of the NuRD complex including Mi-2 regulate neural gene expression to ensure proper development of the larval nervous system. We find that Mi-2 binding in the genome is dynamic during neuronal maturation and Mi-2 mediated repression of ectopic gene expression is restricted to the early stages of neuronal development, indicating that Mi-2/NuRD is required for establishing stable neuronal transcriptomes during the early stages of neuronal differentiation.

Introduction

Neuronal development involves the transition of multipotent precursor cells into highly specialised functional neurons with distinct morphological and biochemical characteristics. The differentiation of precursor cells into specialised cell-types is accompanied by extensive changes in gene expression. These gene expression changes are underpinned by a dynamic chromatin environment in which nucleosome positioning and histone modifications are altered to ensure appropriate transcriptional responses. Whilst recent studies have provided illuminating descriptions of changes to chromatin accessibility and histone modifications during the process of neuronal differentiation (Aughey et al., 2018; Janssens et al., 2022; Preissl et al., 2018; Ziffra et al., 2021), the chromatin-interacting complexes that affect these changes are not well defined.

The Mi-2/NuRD complex is a multiprotein chromatin remodelling complex that influences gene expression via two separate enzymatic activities; ATP-dependent nucleosome remodelling, and histone deacetylation (Tong et al., 1998; Wade et al., 1998; Xue et al., 1998; Zhang et al., 1998). These enzymatic activities are mediated by enzymes which are found in two distinct subcomplexes. The nucleosome remodelling subcomplex contains Mi-2 – a well conserved ATP-dependent nucleosome remodeller (sometimes known as CHD4 in mammals). The second subcomplex is characterised by its histone deacetylase activity. NuRD components are widely conserved and broadly expressed in most metazoan tissues, reflecting the important role of the complex in gene regulation. NuRD complexes have been reported to have critical roles in various developmental processes, for example, in muscle (Gomez-Del Arco et al., 2016) and hematopoietic (Yoshida et al., 2008) cell differentiation. NuRD is also involved in the regulation of the reprogramming of pluripotent cells (Rais et al., 2013).

Mi-2/NuRD complexes are known to have critical roles in neurodevelopment and have been implicated in the aetiology of neurodevelopmental disorders (Hoffmann and Spengler, 2019). A recent study showed that Mi-2 is required in *Drosophila* neuronal lineages to deactivate notch responsive stem-cell enhancers in neuronal progeny, thereby ensuring the fidelity of differentiated cell fate in neurons (Zacharioudaki et al., 2019). Similarly, NuRD was shown to deactivate gene expression by its action on promoters of presynaptic genes to promote synaptic connectivity (Yamada et al., 2014). These studies suggest a predominantly suppressive role for NuRD in the regulation of gene expression. Whilst this is consistent with early models of NuRD activity as a repressive complex, more recent studies have presented a more nuanced role for NuRD in modulating gene expression, which may be neither activating or repressive, but acting to fine tune gene expression and reduce transcriptional noise (Bornelov et al., 2018; Burgold et al., 2019; Ragheb et al., 2020). Therefore, an important unanswered question is whether NuRD is primarily repressive in neuronal development, or whether it may facilitate control of active gene expression as demonstrated in stem cell models.

In mice, NuRD composition is dynamic in cortical development, with alternate Mi-2/CHD paralogues incorporated to mediate distinct effects in different developmental stages (Nitarska et al., 2016). In *Drosophila* the components of the NuRD complex are well conserved, (although only single homologues of most NuRD proteins are identified). However, despite the strong conservation of NuRD's constituent proteins, and ample evidence for physical interactions between them (Reddy et al., 2010; Zhang et al., 2016), the extent to which the canonical NuRD complex regulates gene expression in *Drosophila* is uncertain. A smaller complex consisting of only Mi2 and MEP-1 (termed dMec), has been suggested to be more prevalent than NuRD in fly, and that this complex is responsible for the majority of Mi-2 dependent phenotypes (Kunert et al., 2009). This observation has not been corroborated by further studies, however, NuRD-independent roles for Mi-2 have been suggested to play a role in human cells (Amaya et al., 2013). On the other hand, it is also possible that since NuRD is thought to be comprised of pre-assembled modules (Zhang et al., 2016), and Mi-2 may exist as a peripheral component to the core complex (Low et al., 2016), the detection of non-NuRD associated Mi-2 may simply be a proteomic

artefact that does not reflect a *bona fide* biological activity. Therefore, the functional role of dMEC, and its relationship to the canonical NuRD holocomplex, remains poorly characterised.

Here, we set out to better understand the influence of Mi-2/NuRD complex on gene expression in the development of the central nervous system. We find that knockdown of Mi-2 in larval neurons results in defective optic lobe development as well as ectopic expression non-neuronal genes. We find that Mi-2 represses lineage-inappropriate gene expression independently of NuRD, whilst optic lobe phenotypes are phenocopied by other members of the NuRD complex. Genomic profiling with Targeted DamID revealed distinct binding of Mi-2 containing complexes indicating a repressive role for Mi-2 outside of the canonical NuRD complex. We find that Mi-2 is not required for repression of non-neuronal genes after the early stages of differentiation, indicating that Mi-2 activity is critical for ensuring maintenance of the neuronal gene expression programme during maturation, but alternative mechanisms may be employed in fully differentiated neurons.

Results

Mi-2 is required in neurons for survival and larval locomotion.

Mi-2 has previously been shown to have a role in protecting neural lineages from mitogenic notch signalling, indicating that NuRD has an important role in gene regulation in the neuroblasts and early progeny of *Drosophila* CNS lineages. To better understand the role of NuRD in the fly CNS, we initially set out to examine the distribution of the core ATP-dependent nucleosome remodelling subunit Mi-2. We utilised a MiMIC insertion line in which RMCE results in EGFP-tagged Mi-2 at its endogenous locus (referred to as *Mi-2-GFP* hereafter). We observed that Mi2 appears to be ubiquitously present in the developing third instar larval central nervous system (Figure 1A). GFP signal was clearly visible in nuclei of neural stem cells (NSCs) and progenitor cells (ganglion mother cells (GMCs)), as well as all neurons, with progeny cells (GMCs/newly born neurons) adjacent to NSCs exhibiting particularly high expression (Figure 1B). The ubiquitous nuclear expression of Mi-2 in the larval brain suggests that Mi-2 activity is likely to be involved in gene regulation in all stages of neuronal differentiation, including differentiated neurons,

To understand the importance of *Mi-2* expression in neurons, we used RNAi interference (RNAi) to induce cell-type specific knockdowns of *Mi-2* in the central nervous system. An RNAi line targeting Mi-2 was previously shown to produce robust knockdown of Mi-2 in neuronal lineages, therefore, we decided to utilise this line for our study (Zacharioudaki et al., 2019). Using the pan-neuronal *elav*-GAL4 driver we observed lethality during late larval/pupal stages (Figure 1C). Whilst neuronal *Mi-2* appeared dispensable for embryogenesis and larval survival (possibly due to maternal contribution of Mi-2), we observed a severe mobility defect in larval crawling compared to controls (Figure 1D) indicating that *Mi-2* activity in neurons is required throughout development at all life-stages for normal CNS function.

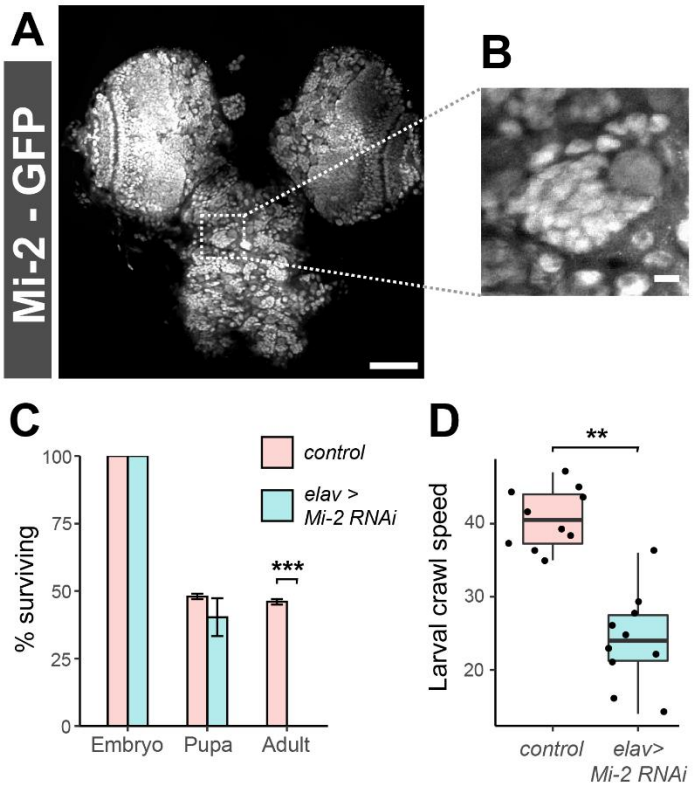

Figure 1. Critical role of *Mi-2* RNAi in *Drosophila* neurons. A) Third instar larval CNS of *Mi-2* GFP-trap line (scale bar = 50 µm). B) Increased magnification of region shown in A. Mi-2 GFP appears highly abundant in progeny cells proximal to neuroblast (scale bar = 5 µm). C) Survival of *Mi-2* RNAi and control (*mCherry-RNAi*) flies during development (**** p < 0.001).* D) Larval crawl speed (cm/minute) in *Mi-2* RNAi and *mCherry* RNAi controls (** p < 0.01).

_Mi-2_ knockdown results in misexpression of non-CNS genes.

To determine the effect of Mi-2 loss on gene expression in neurons of the developing CNS, we performed RNA-seq on larval brains in which *Mi-2* had been knocked down in neurons by RNAi, and compared to controls in which RNAi targeting mCherry was expressed using the same *elav*-GAL4 driver. We found good correlation between replicates (Figure 2 – figure supplement 1A, B) and observed that the expression of *Mi-2* itself was found to be significantly downregulated (Figure 2 – figure supplement 1C) in agreement with previous studies (Zacharioudaki et al., 2019). We found that knockdown of *Mi-2* resulted in significantly more upregulated genes than downregulated (397 downregulated vs 1467 upregulated) indicating that in the context of developing neurons, *Mi-2* has a significant role in the repression of gene expression (Figure 2A-C). Gene ontology (GO) analysis of these significantly up-regulated genes revealed enrichment of GO-terms that may be associated with neuronal maturation or function, such as "ion transport", "sensory perception" and "cell projection assembly" (Figure 2D). However, we also saw enrichment for unexpected terms such as "cilium assembly" that are not typically associated with nervous system development or function.

Closer inspection of the top up-regulated genes revealed the presence of ectopically expressed genes that are usually expressed in non-CNS tissues such as the germline. For example, *vasa* (a well-characterised ovarian germline marker) expression was (~3.5 log2 fold-change) increased compared to controls (Figure 2B). Similarly, *gammaTub37C* – a female germline specific isoform of tubulin, was also very highly upregulated (Figure 2A and Figure 2 – figure supplement 2A, C), as well as *RpS5b*, encoding a germline specific ribosomal protein (Figure 2 – figure supplement 2B, C). We also saw evidence of

male-germline specific genes being upregulated, for example *CG15446* (a transcription factor with testis specific expression) was expressed at much higher levels than controls (Figure 2A). Comparison to tissue-specific transcriptomes indicates that the upregulated genes are usually expressed outside the larval nervous system from a broad range of tissues, including a large cluster of genes that have testis-enriched expression, as well as ovary, fat body, and digestive system (Figure 2E and Supplementary figure 2, – figure supplement 3A, B).

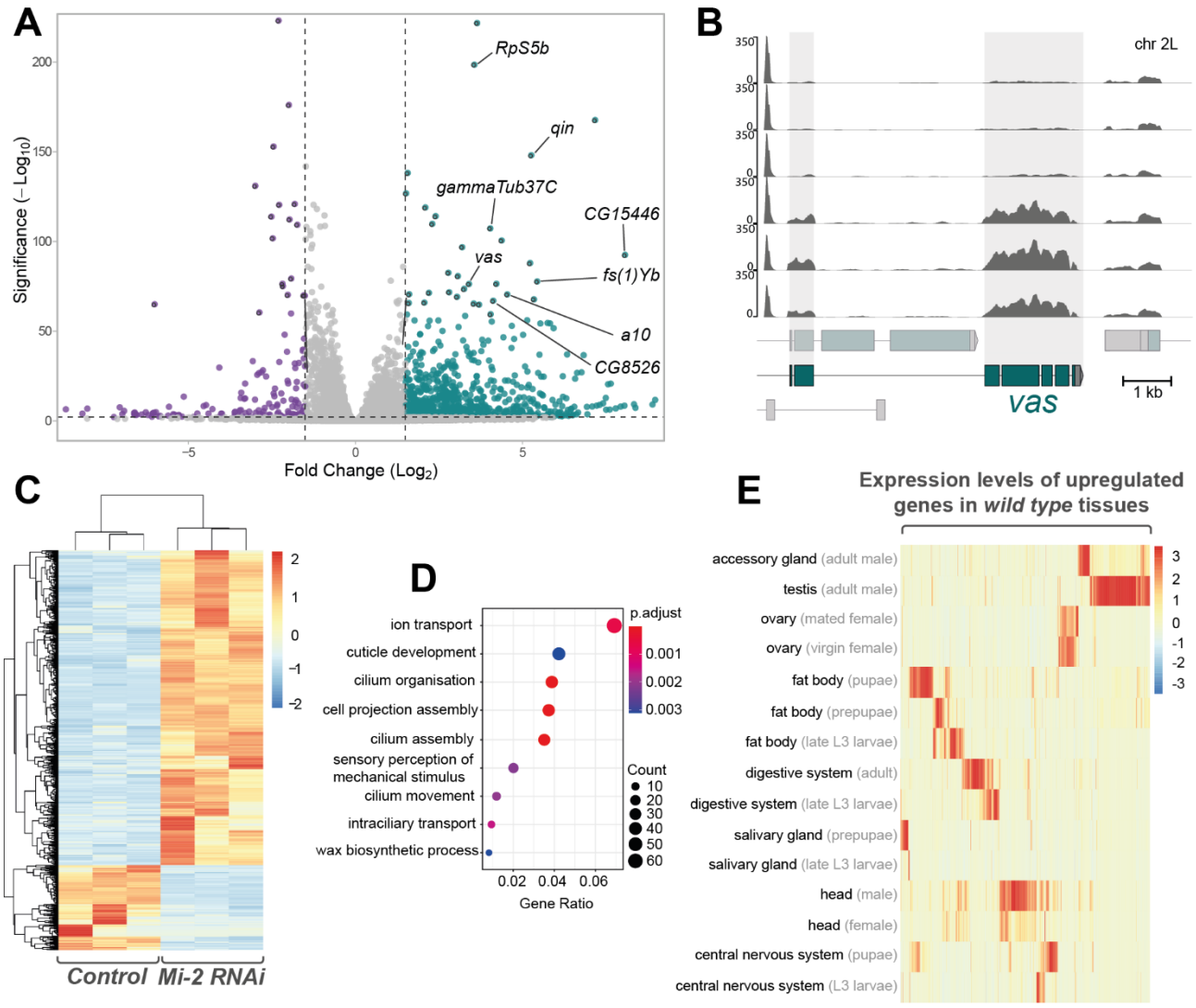

Figure 2. ***Mi-2 knockdown in larval neurons results in extensive gene expression changes.*** A) Volcano plot showing significantly up-regulated (green) and down-regulated (purple) genes with fold-change. Selected mis-expressed genes are annotated. B) RNA-seq tracks showing *vas* mRNA expression in third instar larval CNS (Y-axis is RPKM). C) Heatmap showing relative changes in normalised read-counts between *Mi-2* RNAi and control replicates for all significantly differentially expressed genes (p-adj < 0.05, log2 fold change >1 or <-1). Significantly more genes are upregulated (1467) than downregulated (397). D) Enriched gene ontology terms for genes that are upregulated in *Mi-2* RNAi knockdown. E) Heatmap showing relative expression levels of upregulated genes across selected *Drosophila* tissues (full version in Figure 2 – figure supplement 3A).

138 We also observed misexpression of neuronal lineage specific genes that are not usually highly expressed
139 in the larval central nervous system but are expressed in specific neuronal populations in the adult
140 nervous system. For example, the critical circadian regulator *period* is usually expressed in specific
141 neuronal populations in mature neurons in adult heads with expression being much lower in the larval
142 central nervous system. In *Mi-2* knockdown neurons, *period* was highly upregulated compared to
143 controls. Similarly, the antennal gene *a10* was seen to be very highly upregulated upon knockdown of
144 *Mi-2* in the larval CNS despite usually having expression restricted to the antennae in adult flies (Figure
145 2A and Figure 2 – figure supplement 2C). Therefore, these data indicate that Mi-2 is required to ensure
146 fidelity of neuronal transcriptomes by suppressing expression of spatially and temporally inappropriate
147 genes.

148 ***Mi-2* Knockdown in neurons causes severe optic lobe growth defects.**

149 Performing GO analysis for down-regulated genes indicated enrichment of multiple terms related to cell
150 division and stem cell function (Figure 2 - figure supplement 2C). This is surprising since we knocked
151 down *Mi-2* in neurons, which are exclusively post-mitotic and do not express genes related to cell-
152 division– therefore it is unlikely that Mi-2 could directly downregulate the expression of these genes. To
153 further understand the consequences of *Mi-2* depletion in neurons, we examined dissected third instar
154 larval brains using confocal microscopy. We found that in *Mi-2* knockdown resulted in severe optic lobe
155 defects. Mi-2 knockdown brains were smaller, and it was evident that all recognisable optic lobe
156 structures (including inner and outer optic proliferation centres as well as differentiating medulla and
157 lamina neurons) were found to be completely absent (Figure 3A,B). Interestingly, this included
158 proliferative cells of the optic lobes and neuroepithelium, including the neuroblasts, suggesting that *Mi-*
159 *2* knockdown in neurons causes a non-cell-autonomous effect on the precursor cells of the optic lobes.
160 Therefore, we attributed the enrichment of GO terms relating to precursor cell function to the fact that
161 a large number of cells expressing these genes were not present in the tissue from which RNA was
162 extracted. Due to this severe phenotype in which a large fraction of optic lobe cells are absent, we
163 decided that we could not reliably identify genes that were downregulated as a consequence of Mi-2 loss
164 rather than due to absence of cells expressing those genes. However, since we still saw far fewer
165 downregulated than upregulated genes, this reinforces our conclusion that Mi-2 appears to be mainly
166 acting to suppress gene expression in this context.

167 Since it has previously been reported that *elav*-GAL4 may drive some expression in embryonic glial cells
168 (Berger et al., 2007), we questioned whether unwanted aberrant glial knockdown of *Mi-2* may have
169 resulted in a disruption of signalling that maintains the optic lobe stem cells. To address this, we
170 repeated the *Mi-2* knockdown with an *elav*-GAL4 driver combined with *repo*-GAL80, to repress
171 unwanted expression of the RNAi hairpin in glial cells. In these animals, we observed the same severe
172 optic lobe phenotype as previously with *elav*-GAL4 alone, confirming that neuronal *Mi-2* activity is

173 required for the maintenance of the developing optic lobe in a non-cell-autonomous manner (Figure 3 -
174 figure supplement 1A, B).

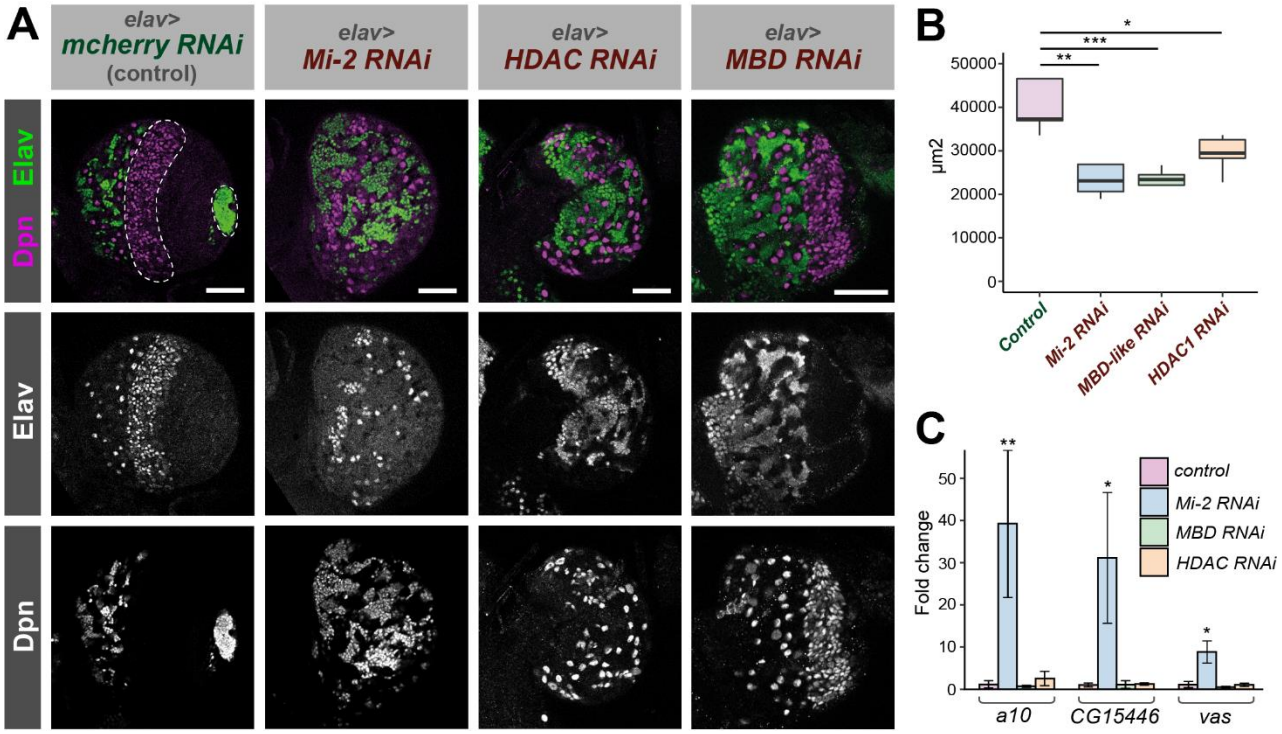

175

Figure 3. *Mi-2* knockdown in neurons causes severe optic lobe development phenotype.
A) Representative images of control (*elav*-GAL4*; ; mCherry*^{RNAi}), *Mi-2* knockdown, *HDAC1* knockdown and *MBD-like* third instar larval CNS (all scale bars = 10 µm). Optic lobe neuroblasts are highlighted by dashed line in control brain. B) Quantification of optic size (µm^2) of genotypes shown in panel A. 8 brains measured for each genotype. C) Quantification of candidate gene expression (selected from upregulated genes in RNA-seq data) in knockdown genotypes.

176

177 ***Mi-2* represses ectopic gene expression independently of histone deacetylation**

178 Having seen significant upregulation of germline and other non-stage or tissue appropriate genes upon
179 *Mi-2* knockdown, we used qPCR to confirm upregulation of a selection of highly mis-expressed candidate
180 genes in *Mi-2* knockdown flies (Figure 3C). Since RNAi mediated knockdowns have previously been
181 associated with off-target effects, we also repeated these qPCR experiments with a second RNAi line
182 which recapitulated the upregulation of ectopic genes previously observed (Figure 3 - figure
183 supplement 2).

184 Since NuRD mediates two distinct enzymatic activities, we first asked whether the histone deacetylase
185 subunit *HDAC1* (also known as *Rpd3*) was required for repression of ectopic genes. We found that
186 depletion of *HDAC1* by RNAi in neurons resulted in lethality during pupal stages similarly to *Mi-2.*
187 However, *HDAC1* knockdown with two independent RNAi lines had no effect on expression of genes that
188 were upregulated upon *Mi-2* knockdown, indicating that whilst neuronal *HDAC1* is essential for survival,

189 histone deacetylation is not required for repression of *Mi*-2 induced ectopic gene expression in larval
190 neurons (Figure 3C and supplementary figure 2).

191 Whilst physical interactions between Mi-2 and most members of the NuRD complex have been reported,
192 previous studies have suggested that *Mi-2* may act independently of the canonical NuRD holocomplex
193 in some contexts (Amaya et al., 2013; Kunert et al., 2009). Therefore, we questioned whether the
194 expression of ectopic genes in *Mi-2* knockdown was dependent on NuRD (albeit without HDAC activity)
195 or mediated by Mi-2 via NuRD-independent mechanisms. To address this, we knocked down *MBD-like,*
196 a core NuRD component thought to bridge the nucleosome remodelling and histone deacetylation
197 subunits. In *MBD-like* RNAi knockdown neurons, no difference in gene expression of ectopic target genes
198 was observed (Figure 3C), providing further evidence of *Mi-2* acting independently of NuRD to mediate
199 gene repression.
200 Having seen NuRD independent effects of *Mi-2* on gene expression, we expected that knockdown of
201 other NuRD complex components would not phenocopy the optic lobe phenotype we observed when
202 *Mi-2* knocked down in neurons. However, we observed that in *HDAC1* and *MBD-like* knockdowns, the
203 larval CNS displayed a similar optic lobe defect to that of *Mi-2* (Figure 3A). Quantification of brain lobe
204 size indicated that *MBD-like* had significantly smaller brain lobes (Figure 3B), however the phenotype
205 was less severe with a small number of optic lobe neuroblasts being present in most brains. MTA1-like
206 is a core component of the NuRD histone deacetylase subcomplex, with cells lacking MTA orthologues
207 in mammals considered to be effectively NuRD-null (Burgold et al., 2019). The severe optic lobe
208 phenotype was also observed when MTA1-like knocked down by cell-specific targeted degradation
209 using the degradFP system (Caussinus et al., 2011) (Figure 3 - figure supplement 3A, B). Therefore, we
210 concluded that whilst *Mi-2* functions to repress some ectopic genes in a NuRD independent manner, its
211 effect on optic lobe development is largely mediated via NuRD. Conversely, the ectopic upregulation of
212 genes is independent of NuRD/histone deacetylation, and does not contribute to optic-lobe
213 developmental defects.

214 **Mi-2 association with chromatin reveals the presence of distinct complexes**

215 Our data, along with previous reports, suggest that more than one Mi-2/NuRD complex species may be
216 present and imparting distinct effects on target loci. To further investigate this, we profiled the genomic
217 binding of NuRD complex components using Targeted DamID (TaDa) (Southall et al., 2013). This
218 approach involves fusing the protein of interest to Dam methylase and expressing in a defined cell
219 population, followed by enrichment and sequencing of selectively methylated regions which reflect loci
220 at which the protein associates with DNA (reviewed in (Aughey et al., 2019)).

221 We used Targeted DamID to profile genomic association of Mi-2 as well as NuRD components MTA1-
222 like and HDAC in neurons (defined by *elav*-GAL4 expression) in the larval CNS. We also assayed for
223 genomic binding of MEP-1, previously reported to associate exclusively with Mi-2 as part of the dMEC
224 complex. Principal component analysis of these data revealed one cluster that included Mi-2 and MEP-

1 replicates, whilst the remaining NuRD components, MTA1-like and HDAC1, appeared to be distinct (Figure 4A, B and D). The close similarity between Mi-2 and MEP-1 binding is further supported by the close correlation seen between the two datasets (pearson R^2 = 0.94/0.95), which is almost as strong as that seen between replicates (Figure 4 - figure supplement 1). In contrast, both MTA-1like and HDAC1 showed relatively poor correlations to MEP-1 or Mi-2, whereas their correlation with each other was slightly stronger. Whilst HDAC1 binding may be expected to be poorly correlated with Mi-2 due to the inclusion of HDAC1 in protein complexes other than NuRD (e.g. with Polycomb Group proteins (Tie et al., 2001)), the relatively low correlation with MTA1-like points towards the possibility of distinct Mi-2 containing complexes having distinct binding in neurons.

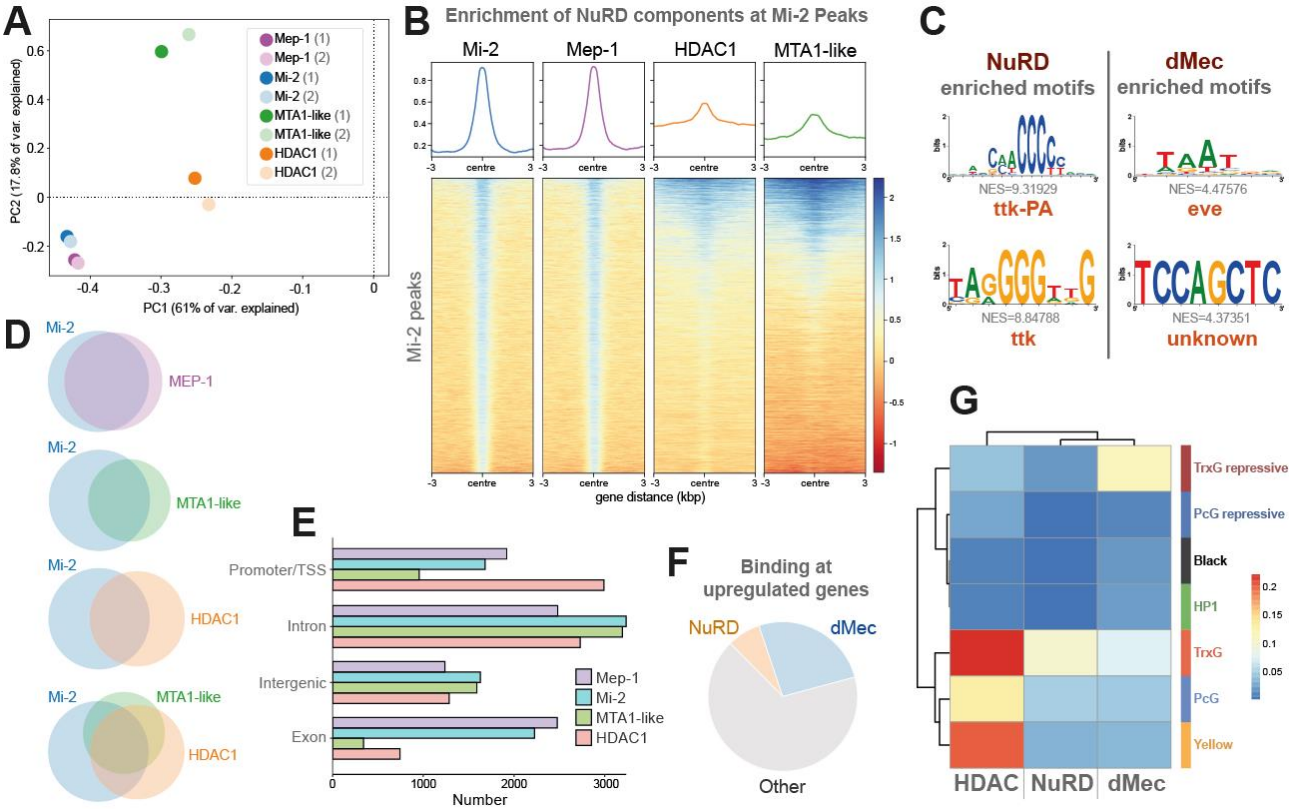

Figure 4. Genomic binding of NuRD components A) Principal component analysis of all NuRD component binding in neurons including replicates. Mi-2/MEP-1 (blue/purple) cluster independently of MTA1-like (green) and HDAC1 (orange) reflecting greater similarity in their binding profiles. B) Heatmap and enrichment plots indicating binding at Mi-2 peaks. C) Top enriched motifs at NuRD and dMec peaks. D) Venn diagrams indicating amount of overlapping peaks between NuRD subunits. All intersections between peaks occur at statistically significant frequencies (Fisher's exact test $p < 10^{-24}$). E) Peak annotation for Mi-2, MEP-1, MTA-1like and HDAC1 peaks. F) Proportion of differentially upregulated genes that directly intersect with Mi-2, MEP-1, MTA-1like and HDAC1 peaks, and differentially upregulated genes intersecting with exclusively Mi-2/MEP-1 or all NuRD subunits. G) Heatmap indicating jaccard similarity statistic between chromatin states and NuRD peaks (Mi-2, MEP-1, MTA-1like and HDAC1) and dMEC (Mi-2 and MEP-1 only), or HDAC peaks.

235 To further understand the relationship between Mi-2 and other NuRD components at the chromatin
236 level, Mi-2 significantly-bound peaks were compared to those of MEP-1, MTA1-like and HDAC1. We
237 found that the majority of MTA1-like peaks coincided with Mi-2, although a significant number of Mi-2
238 peaks did not overlap with MTA1-like (Figure 4D). We observed strong binding of HDAC1 throughout
239 the genome, however, a relatively low proportion of HDAC1 peaks intersected with Mi-2 peaks (Figure
240 4B, D), indicating that Mi-2 is found in association with chromatin without HDAC1 or MTA1-like at the
241 majority of loci.

242 We observed that around half of Mi-2 peaks coincided with either MTA1-like or HDAC1 with fewer still
243 having all three detected at the same site (around a quarter of total Mi-2 peaks). We also saw that a
244 smaller proportion of HDAC1 peaks were shared with Mi-2 compared to MTA1-like presumably due to
245 the inclusion of HDAC1 in other chromatin modifying complexes (Figure 4D). We also observed some
246 MTA1-like peaks that did not overlap with Mi-2 or HDAC1, suggesting that MTA1-like may have
247 undefined roles outside of NuRD. As previously indicated, MEP-1 and Mi-2 peaks intersected at almost
248 all loci. Inspection of the genomic features at which the various peaks were found to bind demonstrated
249 further disparity between Mi-2/MEP-1 and MTA1-like/HDAC1. We found that whilst HDAC1 was found
250 to be enriched at promoters and TSS, Mi-2 and MEP-1 were comparatively enriched in gene bodies,
251 particularly in exons (Figure 4E). Together these data suggest that multiple Mi-2 containing complexes
252 interact with chromatin in neurons, that may or may not possess histone deacetylase activity. In line
253 with previous reports, we refer to sites bound by Mi-2 and MEP-1 as "dMEC" hereafter (Kunert et al.,
254 2009), whilst sites with significant binding of all four profiled components are considered "NuRD" target
255 sites.

256 **dMec and NuRD regulate different genes in neuronal differentiation.**

257 Having seen that Mi-2/NuRD components are distributed unequally in the genome, we examined how
258 binding of NuRD components related to the differentially upregulated genes we found in our RNA-seq
259 experiment. Since previous reports have suggested that dMEC has a role in suppressing ectopic gene
260 expression in cultured cells, we questioned whether this complex may also play a greater role in
261 repressing ectopic gene expression in neurons. We found that NuRD binding (i.e. significant binding of
262 Mi-2, MTA1-like, and HDAC1) was found at a much lower proportion of upregulated genes compared to
263 those bound by dMEC (223 and 797 genes respectively – (Figure 4F)). Along with the different effects
264 seen on gene expression when Mi-2 was knocked down compared to other components, this observation
265 led us to further investigate the role of dMEC in regulating gene expression compared to NuRD.

266 Examining the gene ontology (GO) enrichment of genes bound by either NuRD or dMec revealed clear
267 differences in the processes that were regulated by each complex. We found that NuRD-regulated genes
268 were enriched for GO terms related to organismal development, with "central nervous system
269 development" amongst the top enriched terms. In contrast, genes with dMec peaks were enriched for
270 terms relating to cilia function (Figure 4 - figure supplement 2) reflecting the prevalence of genes that

271 are usually enriched in testis and not expressed in the central nervous system (although it should be
272 noted that it is possible that some of these genes may also be expressed in fully differentiated sensory
273 neurons). Terms relating to synaptic function were also enriched for genes bound by dMEC, which may
274 be expected of a group of genes the expression of which is regulated in neurons. However, inspection of
275 the genes comprising these categories reveals that many of these genes are expressed post-synaptically
276 outside the CNS (*GluRIIA, GluRIIC*) or in later stage pupal CNS in which neurons are in a more
277 differentiated state (e.g. *slo, Syt12*). These results are consistent with a model in which dMEC is largely
278 responsible for repression of ectopic gene activity, whilst NuRD is involved in coordinating appropriate
279 transcription of neuronal genes.

280 We examined NuRD and dMec bound sequences for enrichment of sequence motifs to see if we could
281 identify potential cofactors that may be involved in recruitment or regulation of these complexes. For
282 sequences bound by NuRD, we found that the most highly enriched sequence motifs corresponded well
283 to the consensus sequences for *tramtrack* (*ttk*) (Figure 4C). ttk has previously been shown to interact
284 with MEP-1 to recruit the NuRD complex (Reddy et al., 2010), and physical interactions with other NuRD
285 components have also been reported (Rhee et al., 2014). In contrast, the *ttk* motif was not enriched for
286 sequences covered by dMEC peaks. Instead, the most highly enriched motif identified was a Hox-like
287 motif corresponding most closely to the transcriptional repressor *even-skipped* (*eve*). The differences in
288 the underlying sequences present at NuRD and non-NuRD Mi-2 binding sites suggest that these
289 complexes maybe recruited to target loci by distinct molecular factors.

290 To gain further insight into how Mi-2 containing complexes regulated gene expression we compared
291 binding to the state of the underlying chromatin. Chromatin can be grouped into discrete states
292 reflecting the occupancy of key regulatory proteins (Filion et al., 2010). We compared the binding of
293 HDAC1, Mi-2, MEP-1 and MTA1-like with published data describing chromatin state domains based on
294 a seven-state model (Marshall and Brand, 2017). We found that HDAC1 binding was associated with
295 broadly permissive chromatin states (Figure 4G). Whilst histone deacetylase activity has been thought
296 to be associated with repression of gene expression, these observations are consistent with previous
297 reports that have described enrichment of HDAC binding at active promoters (Wang et al., 2009).
298 Indeed, we also observe strong enrichment of HDAC1 binding at transcription start sites (TSS) as
299 previously reported (Figure 4 – Figure supplement 3). In contrast, Mi-2, MEP-1 and MTA1-like were
300 found to be associated with a mixture of permissive and repressive states, in particular with Trithorax-
301 like permissive and repressive states (Trx-G / Trx-G_repressive). Taking into consideration only regions
302 that are bound by either Mi-2/MEP-1 (dMEC), HDAC alone, or all four proteins (i.e. NuRD), we saw that
303 whilst NuRD showed the greatest similarity to the Trithorax-like permissive state, Mi2/dMEC more
304 strongly coincided with the transcriptionally silent Trithorax-associated repressive state, which is
305 characterised by the presence of Brahma as well as H1 linker histone. These observations support a
306 model in which NuRD independent Mi-2 binding largely mediates gene silencing/repression, whilst
307 NuRD is involved in the regulation of actively expressed genes.

308 **Fully differentiated neurons do not require Mi-2 for silencing of ectopic gene expression or optic**
309 **lobe survival**

310 Previous studies have shown that factors involved in the maintenance of neuronal transcriptomes
311 during early neuronal maturation can have less severe phenotypes in fully differentiated neurons in
312 which synapses have been formed (Hassan et al., 2020; Southall et al., 2014). This correlates with
313 observed changes to the underlying chromatin landscape which is dynamic during differentiation and
314 neuronal maturation (Aughey et al., 2018; Marshall and Brand, 2017). Notch induced hyperplasia in
315 neuronal lineages is enhanced by the knockdown of *Mi-2*, however, this effect is diminished as cells
316 become more differentiated (Zacharioudaki et al., 2019). In our previous knockdown experiments, we
317 employed the *elav*-GAL4 driver to target all neurons in the *Drosophila* larval CNS. This includes a
318 substantial proportion of neurons that are post-mitotic cells, but not fully differentiated to the point at
319 which synaptic proteins are expressed. In fact, it has been suggested that the majority of larval brain
320 *elav*-expressing neurons contribute relatively little to neuronal function (Eichler et al., 2017), since they
321 do not possess axons or dendrites or express ion-channels associated with neurotransmission
322 (Ravenscroft et al., 2020), despite comprising a large proportion of the total cells in the larval brain (Jiao
323 et al., 2021). Furthermore, we observed higher expression of GFP-tagged Mi-2 in newly derived progeny
324 of progenitor cells in the larval CNS, suggesting a potential difference in activity during the early stages
325 of differentiation (Figure 1B). Therefore, we questioned whether Mi-2 dependent optic lobe phenotypes
326 or de-repression of silenced genes would be observed when Mi-2 was knocked down in either earlier or
327 later stages of neuronal differentiation.

328 First, we used *wor*-GAL4, to drive *Mi-2* RNAi in neural stem cells (NSCs). Surprisingly, we found that *Mi-*
329 *2* knockdown in NSCs showed no apparent defects in optic lobe development, with brain lobes having
330 similar sizes to controls (Figure 5A and Figure 5 supplement 1A). In contrast to when *Mi-2* was depleted
331 in neurons (Figure 1D), loss of *Mi-2* in neuroblasts did not result in larval locomotion defects (Figure 5
332 - figure supplement 2). However, *Mi-2* knockdown in neuroblasts did result in increased larval lethality,
333 with very few animals surviving to adulthood (data not shown). Therefore, since brain size, morphology
334 and movement are normal in these animals, these results suggest that Mi-2 is not required for stem cell
335 division or differentiation into neurons. Nevertheless, Mi-2 function in neuroblasts is required for the
336 correct functioning of subsequently born neurons. The lack of optic lobe phenotypes observed in *wor-*
337 GAL4 knockdowns also further underlines that non-cell-autonomous optic lobe phenotypes originate
338 from neuronal depletion of Mi-2.

339 Next, we examined brains in which *Mi-2* RNAi was driven with *nSyb*-GAL4 which is exclusively expressed
340 in more mature synapse forming neurons. In contrast to knockdown in all neurons including immature
341 neurons with *elav*-GAL4, depletion of *Mi-2* exclusively in mature neurons did not produce overt
342 morphological phenotypes and no significant difference in optic lobe area was detected when compared
343 to controls (Figure 5A and Figure 5 supplement 1B). As with the other drivers used, *Mi-2* knockdown

with *nSyb*-GAL4 resulted in lethality during pupal stages. Therefore, whilst Mi-2 is still required in mature neurons, the morphological defects observed are restricted to a critical window of early neuronal maturity.

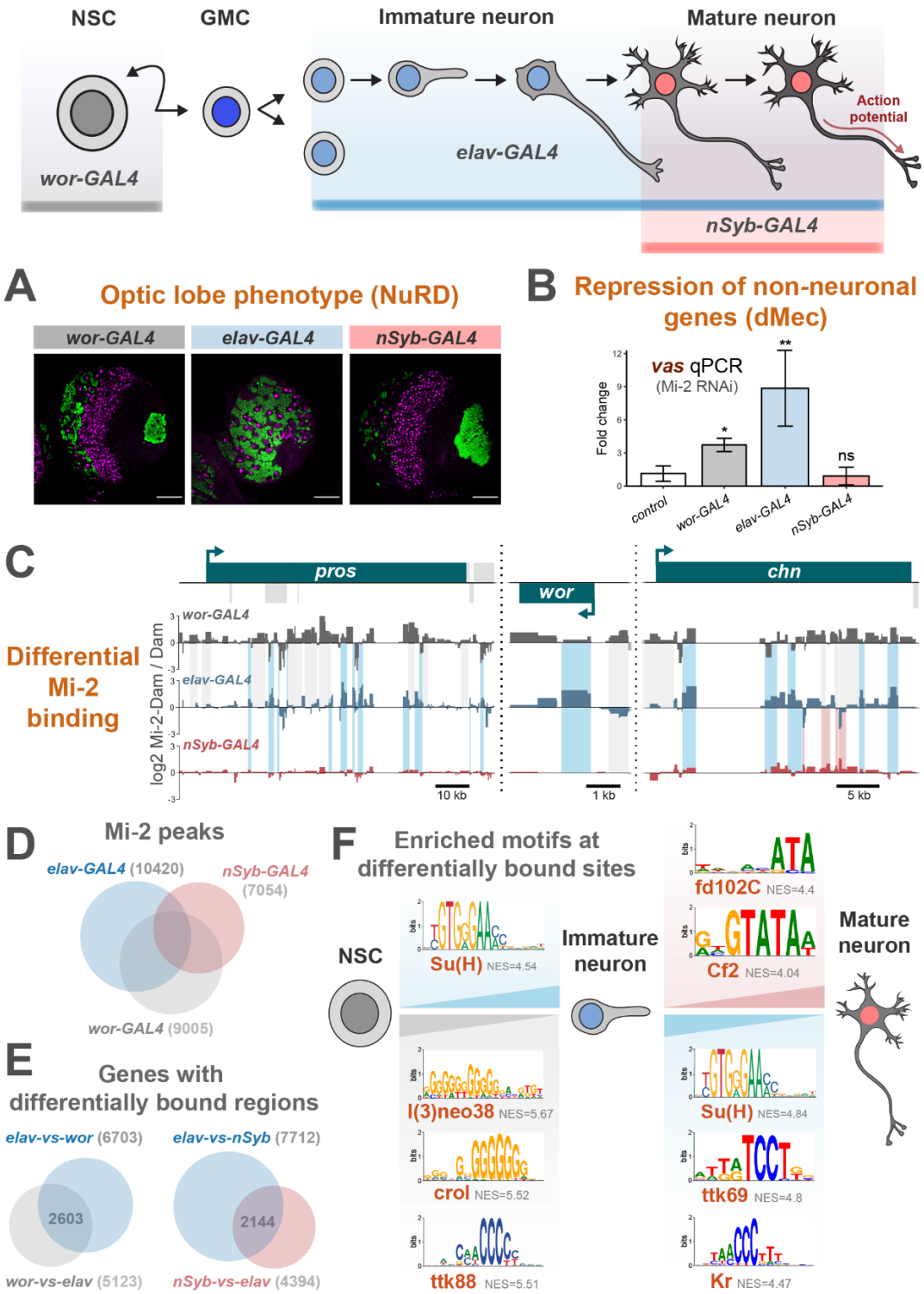

Figure 5. Differential requirements and binding of Mi-2 during neuronal differentiation. A) Larval brain optic lobe morphology when *Mi-2* is knocked down at different stages of differentiation. B) Ectopic expression of *vas* when *Mi-2* is knocked down at different stages of differentiation. C) Examples of differential genomic binding of Mi-2 at neural genes. D) Overlap of Mi-2 binding peaks in NSCs, immature neurons and mature neurons. E) Number and overlap of genes with differential Mi-2 binding. F) Motif analysis of differentially bound regions

371 Since we observed differences in the severity of observed phenotypes resulting from *Mi-2* at different
372 developmental stages, we questioned whether Mi-2 was also required for suppression of ectopic gene
373 expression in NSCs or precursor cells. Using *wor*-GAL4 to knock down *Mi-2* in NSCs, we performed qPCR
374 to detect changes in gene expression. When *Mi-2* was knocked down in NSCs, the expression of female
375 germline marker *vas* was significantly upregulated (Figure 5B), as previously seen with *elav*-GAL4
376 neuronal knockdowns. *vas* expression was upregulated to a lower extent than when induced with *elav*-
377 GAL4 knockdown (~4 fold increase compared to ~10 fold), however this may be due to the lower
378 number of affected cells expressing *wor*-GAL4 rather than reflecting a difference in the requirement for
379 Mi-2 for repression of *vas* in NSCs.

380 In contrast, knockdown in mature neurons using *nSyb*-GAL4 did not result in any detectable change in
381 *vas* mRNA levels (Figure 5B). We also tested whether depletion of *Mi-2* in adult neurons was sufficient
382 to de-repress *vas* expression using a temperature sensitive GAL80 to de-repress *Mi-2* RNAi in neurons
383 using *elav-GAL4* for a 24 hour period after eclosing. As in third instar larvae, no change in *vas,* expression
384 was detectable in adult heads (Figure 5 - figure supplement 3). We also tested for expression of *a10* and
385 *CG15446*, which also did not show any increased expression in adult neurons, indicating that Mi-2 is
386 only required for the repression of ectopic gene expression in the early stages of neuronal maturation.

387 **Dynamic Mi-2 binding during neuronal differentiation**

388 We reasoned that varying consequences of *Mi-2 loss* at different stages of neuronal differentiation may
389 be reflected by changes to Mi-2 binding in different cell types. To examine how Mi-2 genome occupancy
390 changes as neurons are born and mature, we profiled Mi-2 (using TaDa) in NSCs (*wor*-GAL4) and mature
391 neurons (*nSyb*-GAL4) in the larval CNS.

392 Binding profiles between cell types were compared and regions of differential binding identified (Figure
393 5 C, E). Total neurons (*elav*-GAL4) show the largest number of significantly bound peak regions (10,420),
394 with mature neurons binding 7054 genes (Figure 5D). However, the number of peaks common to each
395 cell type is relatively low. Therefore, Mi-2 binding is highly dynamic during neuronal differentiation.

396 We observed that in many cases, at a single gene, there would be sites with enriched binding in NSCs
397 and a different set of enriched Mi-2 binding sites in immature neurons (Figure 5 C, E). A similar change
398 occurs from immature to mature neurons, with 2144 genes that contain both immature-vs-mature and
399 mature-vs-immature regions of Mi-2 enrichment (Figure 5E and the example of *chn* in Figure 5C).

400 Motif enrichment analysis of the differentially bound regions identified transcription factor binding sites
401 (Figure 5F). Binding sites for l(3)neo38, crol and ttk88 are present in the NSC-vs- immature comparison,
402 suggesting that these sites are occluded in NSCs but available for binding in neural progeny.
403 Interestingly, l(3)neo38 occupies a set of putative neuronal enhancers in the developing embryo and is
404 required for the proper formation of the larval brain (Reddington et al., 2020). l(3)neo38 and crol have
405 both been implicated in the regulation of heterochromatin silencing (Schneiderman, 2010 & Swenson,

406 2016). While ttk88 sites are enriched for binding in NSC-vs-immature neurons, ttk69 sites (a different
407 splice isoform) are enriched in the immature-vs- mature comparison. Finally, fd102C and Cf2 sites have
408 greater Mi-2 binding in mature-vs-immature neurons. Fd102C is an uncharacterised forkhead
409 transcription factor highly expressed in the developing and adult nervous system (Krause et al., 2022)
410 and Cf2 is a zinc-finger factor involved in follicle cell fate and myogenic gene expression (Bagni et al.,
411 2002; Hsu et al., 1996). These data indicate that a dynamic repertoire of transcription factors may direct
412 or be influenced by dynamic Mi-2/NuRD binding during neuronal maturation. It is clear from the broad
413 changes in binding that Mi-2 coordinates a distinct gene expression programme in newly born neurons
414 compared to fully differentiated neurons corresponding to the differences in phenotypic outcomes
415 observed.

416 Su(H) (Notch co-factor) motifs were enriched in both immature-vs-NSC and immature-vs-mature
417 regions (Figure 5F). This aligns with previous work showing that Mi-2 is required to deactivate notch
418 responsive stem-cell enhancers in neuronal progeny (Zacharioudaki et al., 2019). Mi-2 was implicated
419 in the silencing of genes in the *E(spl)-C* locus, with broad binding of Mi-2 across this locus having been
420 demonstrated in *Drosophila* cell lines (Ho et al., 2014; Kreher et al., 2017). Consistent with this result we
421 saw strong binding of Mi-2 across the *E(spl)-C* locus in both NSCs and immature neurons (Figure 5 –
422 figure supplement 4). This study also showed that in more mature neurons Mi-2 depletion was not
423 sufficient to enhance notch-induced overgrowth. We saw no significant binding of Mi-2 in mature
424 neurons across the entire region (approx. 50 kb), supporting the conjecture that in more fully
425 differentiated cells, continued chromatin remodelling of the *E(spl)* genes by Mi-2 is not required for their
426 repression.

427 Discussion

428 Chromatin remodellers are critical regulators of gene expression, however, the factors that regulate
429 their spatial and temporal function in complex tissues *in vivo* during animal development are still poorly
430 understood. Here we demonstrate distinct roles for Mi-2 containing chromatin remodelling complexes
431 in the development of the *Drosophila* larval nervous system. We show that the consequences of Mi-2
432 loss are dependent on developmental context, highlighting the importance of mechanisms that maintain
433 the neuronal transcriptome during early maturation.

434 The NuRD complex was originally thought to be a solely repressive complex (Xue et al., 1998), however
435 it has since been shown that NuRD may have activating or repressive characteristics. In mouse
436 embryonic stem cells (ESCs) NuRD activity was shown to be more nuanced, acting to fine-tune the
437 expression of the genes that it regulates (Bornelov et al., 2018). This may be conducted via local
438 decompaction of chromatin to facilitate enhancer-promoter interactions (Basu et al., 2021).

439 Whilst the function and mechanisms of action of the NuRD holocomplex are becoming better
440 understood, evidence is accumulating pointing towards biological functions for Mi-2 outside of NuRD

441 which are largely unknown. Mi-2 from *Drosophila* or humans is sufficient for the remodelling of
442 nucleosomes *in* vitro, in the absence of other NuRD components (Brehm et al., 2000; Wang and Zhang,
443 2001). In mouse embryos, Mi-2 orthologue CHD4 was shown to be necessary for lineage specification in
444 a manner that was independent of MBD proteins that are required for a functional NuRD complex
445 (O'Shaughnessy-Kirwan et al., 2015). Similarly, loss of CHD4 in human erythroid cells resulted in de-
446 repression of fetal *γ-globin*, which occurred independently of NuRD (Amaya et al., 2013). Furthermore,
447 similarly to what we observe in neurons, MBD3 was found to bind at less than half of all CHD4 sites in
448 mouse ESCs and were anti-correlated to histone markers associated with transcription (Bornelov et al.,
449 2018). Therefore, it is likely that NuRD-independent Mi-2 regulation of gene expression is a conserved
450 feature in animal cells.

451 A previous study concluded that Mi-2 in complex with MEP-1 (dMec) was the dominant Mi-2 containing
452 complex in *Drosophila* Kc cells (Kunert et al., 2009). From this observation it could be inferred that NuRD
453 plays a relatively minor role in the regulation of gene expression. However, this conclusion was drawn
454 based on biochemical interactions and relative stoichiometries of NuRD components. We find that in
455 contrast to the abundance of dMec, we find that around a third of Mi-2 peaks intersect with MTA1-like,
456 indicating that NuRD is prevalent at a large number of loci. Furthermore, severe optic lobe phenotypes
457 were observed with multiple NuRD components, which did not always include de-repression of lineage-
458 inappropriate genes. These data indicate that despite being present at lower amounts than dMec, NuRD
459 plays a critical role in nervous system development. Whilst it is possible that the proportions of
460 NuRD/dMec may differ between the central nervous system and cultured Kc cells, we would suggest
461 that the relative amounts of protein detected by biochemical means is likely not reflective of either the
462 distribution of sites at which complexes are associated in the genome, or the severity of consequences
463 resulting from their loss.

464 The maintenance of transcriptomes in differentiated cells is necessary for the proper functioning of
465 tissues and organs. As some of the most highly specialised and diverse cells in the body, neurons must
466 tightly control gene expression. Previous studies have shown that transcription factors are required to
467 maintain neuronal cell fate. For example, loss of *lola* or *nerfin-1* in *Drosophila* results in de-
468 differentiation of neurons, giving rise to tumours consisting of aberrantly dividing neural stem cells
469 (Froldi et al., 2015; Southall et al., 2014). Similarly, the SWI/SNF complex ensures proper differentiation
470 by preventing lineage reversion in some neural progenitor populations (Eroglu et al., 2014). However,
471 the mechanisms by which non-neuronal genes are repressed in maturing and differentiated neurons are
472 poorly understood. Our data indicates that Mi-2 represses non-neuronal genes such as those normally
473 expressed in the germline, and that this is largely independent of NuRD. Interestingly, Mi-2/dMec was
474 previously shown to repress proneural gene expression in Kc cells (which are derived from embryos)
475 (Kunert et al., 2009), suggesting that Mi-2 may repress ectopic gene expression in multiple tissue types
476 dependent on context. A similar phenotype has also been reported in *C. elegans* in which MEP-1/Mi-2
477 knockdown resulted in expression of germline genes in somatic tissues, indicating that this may be a

478 conserved function of Mi-2 (Unhavaithaya et al., 2002). It is possible that in mammals NuRD-
479 independent CHD4 function is also required for gene repression since loss of CHD4 in lymphocytes
480 results in upregulation of non-hematopoietic genes which is strikingly similar to the upregulation of
481 ectopic genes we see in neurons (Arends et al., 2019). However, it remains unclear whether this
482 transcriptional repression is dependent on histone deacetylase activity /NuRD, or NuRD independent
483 CHD4 activities.

484 Mi-2/CHD4 is frequently mutated in human cancers and high expression is frequently associated with
485 negative outcomes (Forbes et al., 2016). Another feature common to many somatic cancers is the
486 expression of genes that are normally restricted to the germline (sometimes referred to as cancer-testis
487 antigens) (Fratta et al., 2011), and expression of germline genes has been implicated in driving
488 malignant tumour growth (Janic et al., 2010). Given our finding that germline genes are upregulated
489 upon depletion of Mi-2 it is interesting to speculate that there may be a clinically relevant link between
490 mutations in Mi-2/CHD4 and ectopic germline gene expression in tumours.

491 Interestingly, our data show that Mi-2 is only required to suppress ectopic gene expression up to the
492 early stages of neuronal maturation, whereas in more fully differentiated cells it is dispensable
493 (although it is still required for adult survival). Therefore, it is likely that other molecular factors are
494 required for the repression of these genes following synaptogenesis. It is possible to speculate that Mi-
495 2/dMEC is required to establish a stable epigenetic state following recruitment by sequence specific
496 transcription factor binding, after which these states are maintained by separate chromatin modifying
497 proteins or complexes. We previously observed that neuron-appropriate gene expression programmes
498 were maintained by Cap-G, a member of the condensin complex (Hassan et al., 2020). Similarly, with *Mi-*
499 *2* knockdown, less severe phenotypes – and fewer misregulated genes were apparent upon Cap-G
500 depletion, indicating that multiple factors may act to maintain the neuronal transcriptome in early
501 neuronal differentiation. Whether these factors act via related pathways or mechanisms is yet to be
502 determined.

503 The degree of differential binding of Mi-2 observed during neuronal differentiation is quite striking,
504 (both with respect to the extent across the genome, as well as the dynamic changes occurring at single
505 genes), and is consistent with the idea that Mi-2 coordinated a distinct gene expression programme
506 during early neuronal differentiation compared to in mature neurons. Analysis of these regions
507 identified enriched transcription factor binding sites. This suggests that either the cognate transcription
508 factor is recruiting Mi-2 to these sites, or that Mi-2 is independently positioned there to establish an
509 epigenetic state to prevent or to block the binding of the factor. Since it seems that Mi-2 exhibits at least
510 two independent modes of interacting with chromatin (i.e. via dMEC/NuRD), either or both of these
511 models may be true depending on the presence of other subunits and wider genomic context. Su(H)
512 binding sites are found at sites enriched in immature neurons versus both NSCs and mature neurons
513 (Figure 5F). Furthermore, l(3)neo38 binding sites, that have been identified at neural enhancers

514 (Reddington et al., 2020), are more strongly bound in NSCs compared to immature neurons. Therefore,
515 for at least Su(H) and l(3)neo38, Mi-2 appears to be blocking binding of these factors (loci specific) at
516 stages of differentiation where their function is not required/wanted.

517

518 # Materials and Methods

519 **Fly stocks**

520 Unless stated otherwise flies were kept on standard fly food media at 25 degrees. A full list of fly stocks
521 used in this study can be found in Supplement Table 1.

522 **Immunohistochemistry and imaging**

523 Third instar larval CNS were dissected in PBS and fixed for 20 min with 4% formaldehyde in PBS. The
524 following antibodies were used in this study: rat anti-Elav (Developmental Studies Hybridoma Bank),
525 chicken anti-GFP (Thermo scientific), and guinea pig anti-Dpn (kind gift from A. Brand). Samples were
526 imaged using a Zeiss LSM510 confocal microscope and images processed using image J.

527 **Generation of Targeted DamID lines**

528 *MEP-1* and *Mi-2* were amplified by PCR from cDNA with primers including 30 bp complementary
529 sequence to *pUASTattB-LT3-Dam* (Southall et al., 2013) (see Supplement Table 2). Linearised *pUAST-*
530 *LT3-Dam* (digested with NotI and XbaI) was combined with either *MEP-1* or *Mi-2* PCR-amplified coding
531 sequences in a Gibson assembly reaction using NEBuilder® HiFi DNA Assembly kit (NEB) following
532 manufacturers protocols. Resulting N-terminal fusion constructs were injected into *attP2* flies (*y w*
533 *P{y[+t7.7]=nos-phiC31\int.NLS}X #12;; P{y[+t7.7]=CaryP}attP2* – Department of Genetics Microinjection
534 Service, Cambridge) for integration on the third chromosome.

535 *UAS-MTA-1-like-Dam* and *UAS-HDAC1-Dam* were generated using the FlyORF-TaDa cassette exchange
536 protocol as previously described (Aughey et al., 2021). Briefly, *UAS-HDAC1* and *UAS-MTA1-like* FlyORF
537 lines were crossed to *hsFLP; TaDa-FlyORF.* Progeny were heat-shocked at 37 degrees for 45 mins at 96
538 hours following larval hatching. Resulting males were crossed to *Dr/TM6B* and white-eyed F2 males and
539 female virgins used to create a stable stock.

540 **Targeted DamID**

541 Dam fusion or Dam-only males were crossed to virgins of the appropriate driver line for expression of
542 Dam in the desired cell-types. For expression in NBs, all larval neurons (including immature neurons),
543 or mature neurons only - the drivers *wor*-GAL4*; tub*-GAL80^{ts}*, elav*-GAL4*; tub*-GAL80^{ts}*, and nSyb*-GAL4*;*
544 *tub*-GAL80^{ts}, were used, respectively. Embryos were collected for 4 hr then raised at 18°C to prevent
545 premature Dam expression. Animals were transferred to 29°C at 8 days after embryo deposition for 24
546 hours. 60 larval central nervous systems were dissected and stored at -80 degrees. Genomic DNA

547 extraction, methylated DNA enrichment and library preparation were carried out as previously
548 described (Marshall et al., 2016). Two biological replicates were generated for each experiment.

549 Libraries were sequenced with 50 bp single end sequencing on Illumina HiSeq or NovaSeq platforms.
550 >15 million reads were obtained for each library. Data were processed using a previously described Perl
551 pipeline (Marshall and Brand, 2015) (https://github.com/owenjm/damidseq_pipeline).

552 Peak calling was performed using a previously described Perl program (available at
553 https://github.com/tonysouthall/Peak_calling_DamID) which allows for the identification of broadly
554 bound regions that characterise DamID data (Estacio-Gomez et al., 2020). Briefly, false discovery rate
555 (FDR) was calculated for regions consisting of >1 GATC bounded fragments for each replicate.
556 Significant (FDR<0.01%) regions present in all replicates are merged to form a final peak file. Enriched
557 motifs discovery was performed using i-cisTarget on significant peak regions (Herrmann et al., 2012).
558 Intersecting regions for comparison of binding between Mi-2, MEP-1, MTA1-like, or HDAC1 were
559 computed using bedtools intersect utility (Quinlan and Hall, 2010). Similarity between binding peaks
560 was determined using the bedtools jaccard utility, which calculates the ratio between the number of
561 intersecting base pairs and the union between two coordinate sets (Favorov et al., 2012).

562 **Larval crawling assays**

563 Larval crawling assays were conducted as in (Nichols et al., 2012). Briefly, individual third instar
564 wandering larva were placed on room temperature agar with a 10 mm^2 grid placed underneath as a
565 distance reference. Larvae were left to acclimatise for 1 min after which larval movement was tracked
566 visually. Ten animals were used per genotype with three technical replicates performed per animal.

567 **Developmental survival assays**

568 Flies of the appropriate genotype were left in cages containing standard food media supplemented with
569 yeast and left to acclimatise over three nights at 25 °C. Food media was exchanged for apple juice agar
570 and flies left to lay for 5 h. Following the laying period, 100 embryos were transferred to fresh food vials
571 to allow for counting of surviving adults and pupae.

572 **RNA extraction**

573 Three biological replicates were used for knockdown or control samples. Third instar larval CNS were
574 dissected from thirty animals per replicate and total RNA extracted using TRIzol reagent
575 (https://tools.thermofisher.com/content/sfs/manuals/trizol_reagent.pdf) following suppliers
576 protocols. Library preparation and sequencing were subsequently performed by Beijing Genomics
577 Institute (BGI). Sequencing data was mapped to the Drosophila genome (release 6.22) using STAR
578 (Dobin et al., 2013). Mapped files were collected in a matrix using featureCounts from the Rsubread
579 package (Liao et al., 2019). Differential expression analysis and MA plots were carried out using the
580 Deseq2 R package (Love et al., 2014).. Genes that had an adjusted p-value <0.05 and a log2 fold change

581 greater than 1 (for upregulated) or less than -1 (for downregulated) were classified as significant.
582 Heatmap generated using pheatmap package in R. Analysis of tissue specific gene enrichment was
583 performed using DGET (Hu et al., 2017).

584 **qRT-PCR**

585 Following RNA extraction, reverse transcription was performed using the iScript cDNA synthesis kit
586 (Bio-Rad), following manufacturer's protocols. qRT-PCR was carried out using iTaq Universal SYBR
587 Green Supermix (Bio-Rad). Expression of target genes was normalised to *Ribosomal Protein L4* (*Rpl4*)
588 and compared to expression in control samples expressing RNAi targeting *mCherry*. Primers amplifying
589 sequences <200 bp were designed to span exon junctions where possible (sequences used can be found
590 in Supplement Table 2. Three biological replicates were carried out for each genotype, with at least two
591 technical replicates for each biological replicate.

592 **Data availability**

593 All raw sequence files and processed files have been deposited in the National Center for Biotechnology
594 Information Gene Expression Omnibus (GSE199146).

595

596 **Figure Legends**

597 **Figure 1. Critical role of *Mi-2* RNAi in *Drosophila* neurons.** A) Third instar larval CNS of *Mi-2* GFP-
598 trap line (scale bar = 50 µm). B) Increased magnification of region shown in A). Mi-2 GFP appears highly
599 abundant in progeny cells proximal to neuroblast (scale bar = 5 µm). C) Survival of *Mi-2* RNAi and control
600 (*mCherry-RNAi*) flies during development (*** $p < 0.001$, unpaired t-test). D) Larval crawl speed
601 (cm/minute) in *elav*-GAL4 *x Mi-2* RNAi and *elav*-GAL4 *x mCherry* RNAi controls (** $p < 0.01$, unpaired t-
602 test. n = 10 animals per genotype).

603 **Figure 2. *Mi-2* knockdown in larval neurons results in extensive gene expression changes.** A)
604 Volcano plot showing significantly up-regulated (green) and down-regulated (purple) genes with fold-
605 change (compared to *mCherry* RNAi control). Selected mis-expressed genes are annotated. B) RNA-seq
606 tracks showing *vas* mRNA expression in third instar larval CNS (Y-axis is RPKM). C) Heatmap showing
607 relative changes in normalised read-counts between *Mi-2* RNAi and *mcherry* RNAi control replicates for
608 all significantly differentially expressed genes (p-adj < 0.05, log2 fold change >1 or <-1). Significantly
609 more genes are upregulated (1467) than downregulated (397). D) Enriched gene ontology terms for
610 genes that are upregulated in *Mi-2* RNAi knockdown. E) Heatmap showing relative expression levels of
611 upregulated genes across selected *Drosophila* tissues (full version in Figure 2 – figure supplement 3A).

612 **Figure 3. *Mi-2* knockdown in neurons causes severe optic lobe development phenotype.** A)
613 Representative images of control (*elav*-GAL4 *;; mCherry*^{RNAi}), *Mi-2* knockdown, *HDAC1* knockdown and
614 *MBD-like* third instar larval CNS (all scale bars = 10 µm). Optic lobe neuroblasts are highlighted by

615 dashed line in control brain. B) Quantification of optic size (μm^2) of genotypes shown in panel A. 8 brains
616 measured for each genotype. (*P< 0.05, **P < 0.005, ***P < 0.0005, one-way anova with Tukey HSD post-
617 hoc test)C) Quantification of candidate gene expression (selected from upregulated genes in RNA-seq
618 data) in knockdown genotypes. *P< 0.05, **P < 0.005, one-way anova with Tukey HSD post-hoc test.
619 Error bars show standard deviation.

620 **Figure 4. Genomic binding of NuRD components.** A) Principal component analysis of all NuRD
621 component binding in neurons including replicates. Mi-2/MEP-1 (blue/purple) cluster independently
622 of MTA1-like (green) and HDAC1 (orange) reflecting greater similarity in their binding profiles. B)
623 Heatmap and enrichment plots indicating binding at Mi-2 peaks. C) Top enriched motifs at NuRD and
624 dMec peaks with normalised enrichment scores (NES) indicated. D) Venn diagrams indicating amount
625 of overlapping peaks between NuRD subunits. All intersections between peaks occur at statistically
626 significant frequencies (Fisher's exact test $p < 10^{-24}$). E) Peak annotation for Mi-2, MEP-1, MTA-1like and
627 HDAC1 peaks. F) Proportion of differentially upregulated genes that directly intersect with Mi-2, MEP-
628 1, MTA-1like and HDAC1 peaks, and differentially upregulated genes intersecting with exclusively Mi-
629 2/MEP-1 or all NuRD subunits. G) Heatmap indicating jaccard similarity statistic between chromatin
630 states and NuRD peaks (Mi-2, MEP-1, MTA-1like and HDAC1) and dMEC (Mi-2 and MEP-1 only), or HDAC
631 peaks. (N.b. 1= perfect similarity, 0 = no similarity)

632 **Figure 5. Differential requirements and binding of Mi-2 during neuronal differentiation.**

633 A) Larval brain optic lobe morphology when Mi-2 is knocked down at different stages of differentiation.
634 B) Ectopic expression of vas when Mi-2 is knocked down at different stages of differentiation (*P< 0.05,
635 **P < 0.005, one-way anova with Tukey HSD post-hoc test. Error bars show standard deviation). C)
636 Examples of differential genomic binding of Mi-2 at neural genes. D) Overlap of Mi-2 binding peaks in
637 NSCs, immature neurons and mature neurons. E) Number and overlap of genes with differential Mi-2
638 binding. F) Motif analysis of differentially bound regions.

639 Supplementary Figure Legends

640 **Figure 2 – figure supplement 1. RNA-seq quality control.** A) Heatmap and B) scatter plot showing
641 Pearson correlation of RNA-seq reads between biological replicates and control and experimental
642 groups. Very strong correlations are observed between replicates with slightly lower correlations
643 between knockdown and controls reflecting the changes in *Mi-2* RNAi transcriptome. C) Genome
644 browser tracks indicating RNA-seq read coverage at the *Mi-2* locus. *Mi-2* reads are clearly depleted in
645 *Mi-2 RNAi* compared to *elav*-GAL4 *x mCherry RNAi* controls (adjusted p value < 2.2×10^{-227}).

646 **Figure 2 – figure supplement 2. Differentially expressed genes.** A) Read coverage for A)
647 *gammaTub37C* and B) *RpS5b* loci, which are non-CNS genes ectopically expressed in *Mi-2* knockdown.
648 C) Heatmap showing relative changes in normalised gene expression for the thirty most significantly

649 up-regulated genes. D) Heatmap showing relative changes in normalised gene expression for the thirty
650 most significantly down-regulated genes.

651 **Figure 2 – figure supplement 3. Expression of differentially expressed genes in other tissues.** A)
652 Heatmap showing relative expression levels of upregulated genes across all tissues. B) Stacked bar plot
653 showing percentage of upregulated genes that are expressed at different levels in specific tissues. Note
654 that many upregulated genes are expressed at "very low" levels in the fly CNS, whilst upregulated genes
655 are frequently expressed at "moderate" to very high levels in germline and other non-CNS tissues.

656 **Figure 3 – figure supplement 1. Optic lobe phenotype is not due to *Mi-2* knockdown in glial cells.**
657 A) Optic lobe of third instar larvae in which *repo-GAL80* represses glial GAL4 expression. Severe optic
658 lobe growth defect is still observed as in *elav*-GAL4 *; Mi-2 RNAi* brains. Scale bar = 50 μm. B)
659 Quantification of optic lobe area in control (*elav*-GAL4>*mCherry-RNAi*), *Mi-2* knockdown (*elav*-GAL4 >
660 *Mi2-RNAi*), and *Mi-2* knockdown with glial GAL80 expression (*elav*-GAL4 > *Mi-2 RNAi / repo*-GAL80).
661 **P < 0.005, ***P < 0.0005, one-way anova with Tukey HSD post-hoc test. n ≥ 6 animals per genotype.
662 Error bars show standard deviation.

663 **Figure 3 – figure supplement 2. Verification of Mi-2 and HDAC RNAi lines.** qPCR measurement of
664 non-neuronal genes in larval brains using alternative RNAi lines for *Mi-2* and *HDAC*. These confirm the
665 results obtained using the original RNAi lines. **P < 0.005, ***P < 0.0005, one-way anova with Tukey
666 HSD post-hoc test. Error bars show standard deviation.

667 **Figure 3 – figure supplement 3. Knockdown of MTA1-like in neurons using the degradFP system.**
668 A) Control brains lobes (*elav*-GAL4 *; MTA1-like-GFP*) are morphologically normal whilst knockdown of
669 MTA1-like in neurons causes a severe optic lobe defect. Scale bar = 50 μm. B) Quantification of optic lobe
670 area in control (*elav*-GAL4 *; MTA1-like-GFP*), and MTA1-like knockdown (*elav*-GAL4 *; UAS-Nslmb-vhh-*
671 *GFP; MTA1-like-GFP*) ***P < 0.0005 – unpaired t-test, n ≥ 6 animals per genotype..

672 **Figure 4 – figure supplement 1. Quality control for Targeted DamID data.** Correlation between
673 NuRD subunits (including replicates) in larval neurons (*elav*-GAL4). Very strong correlations are seen
674 between Mi-2 and MEP-1 binding while the correlation between Mi-2/MEP-1 and either MTA-1like or
675 HDAC1 are relatively lower. Good correlations are exhibited between replicates for each subunit
676 (spearman's correlation r^2=0.85-0.95).

677 **Figure 4 – figure supplement 2. GO analysis of NuRD and dMec gene targets.** A) GO analysis of NuRD
678 gene targets. B) GO analysis of dMec gene targets genes.

679 **Figure 4 – figure supplement 3. Metagene analysis of HDAC binding.** TSS is Transcriptional Start
680 Site and TES is Transcriptional End Site.

681 **Figure 5 – figure supplement 1. Quantification of larva; optic lobe area in NSC and mature**
682 **neuron Mi-2 knockdowns.** A) Quantification of 3rd instar larval optic lobe area in controls (*wor-*

683 GAL4>*mCherry-RNAi*) and NSC *Mi-2* knockdown (*wor*-GAL4>*Mi-2-RNAi*). B) Quantification of 3rd instar
684 larval optic lobe area in controls (*nSyb*-GAL4>*mCherry-RNAi*) and mature neuron *Mi-2* knockdown
685 (*nSyb*-GAL4>*Mi-2-RNAi*).

686 **Figure 5 – figure supplement 2. Larval crawl speed with Mi-2 knockdown in NSCs.** Larval crawl
687 speed (cm/minute) in *wor*-GAL4 x *Mi-2* RNAi and *wor*-GAL4 x *mCherry* RNAi controls. No significant
688 changes in crawl speed were observed (Unpaired t-test, n = 10 animals per genotype).

689 **Figure 5 – figure supplement 3. Knockdown of *Mi-2* in adult brain neurons does not cause ectopic**
690 **expression of genes.** qPCR measurement of gene expression in adult heads. *Mi-2*^{RNAi} is induced for 24
691 hours using GAL80^{ts}. No significant changes in expression of either *vas, a10,* or *CG15446* were observed
692 (unpaired t-test, error bars show standard deviation).

693 **Figure 5 – figure supplement 4. Mi-2 binding at the E(spl) complex is lost in mature neurons.** Grey
694 boxes represent genes.

695 Acknowledgments

696 We would like to thank the Southall lab and Imperial College fly community for help and feedback on
697 this project. We would like to thank Andrea Brand for generously providing fly stocks and the Dpn
698 antibody. We also thank the Bloomington *Drosophila* Stock Center (NIH P40OD018537) for fly stocks.
699 This work was funded by a Wellcome Trust Investigator grant 104567 to T.D.S and a BBSRC grant
700 BB/P017924/1 to T.D.S. and G.N.A.

701

702

References

Amaya, M., Desai, M., Gnanapragasam, M.N., Wang, S.Z., Zu Zhu, S., Williams, D.C., Jr., and Ginder, G.D. (2013). Mi2beta-mediated silencing of the fetal gamma-globin gene in adult erythroid cells. *Blood* 121, 3493-3501.

Arends, T., Dege, C., Bortnick, A., Danhorn, T., Knapp, J.R., Jia, H., Harmacek, L., Fleenor, C.J., Straign, D., Walton, K.*, et al.* (2019). CHD4 is essential for transcriptional repression and lineage progression in B lymphopoiesis. *Proc Natl Acad Sci U S A* 116, 10927-10936.

Aughey, G.N., Cheetham, S.W., and Southall, T.D. (2019). DamID as a versatile tool for understanding gene regulation. *Development* 146.

Aughey, G.N., Delandre, C., McMullen, J.P.D., Southall, T.D., and Marshall, O.J. (2021). FlyORF-TaDa allows rapid generation of new lines for in vivo cell-type-specific profiling of protein-DNA interactions in Drosophila melanogaster. *G3 (Bethesda)* 11.

Aughey, G.N., Estacio Gomez, A., Thomson, J., Yin, H., and Southall, T.D. (2018). CATaDa reveals global remodelling of chromatin accessibility during stem cell differentiation in vivo. *Elife* 7.

Bagni, C., Bray, S., Gogos, J.A., Kafatos, F.C., and Hsu, T. (2002). The Drosophila zinc finger transcription factor CF2 is a myogenic marker downstream of MEF2 during muscle development. *Mech Dev* 117, 265-268.

Basu, S., Shukron, O., Hall, D., Parutto, P., Ponjavic, A., Shah, D., Boucher, W., Lando, D., Zhang, W., Reynolds, N.*, et al.* (2021). Live-cell 3D single-molecule tracking reveals how NuRD modulates enhancer dynamics. *bioRxiv*, 2020.2004.2003.003178.

Berger, C., Renner, S., Luer, K., and Technau, G.M. (2007). The commonly used marker ELAV is transiently expressed in neuroblasts and glial cells in the Drosophila embryonic CNS. *Dev Dyn* 236, 3562-3568.

Bornelov, S., Reynolds, N., Xenophontos, M., Gharbi, S., Johnstone, E., Floyd, R., Ralser, M., Signolet, J., Loos, R., Dietmann, S.*, et al.* (2018). The Nucleosome Remodeling and Deacetylation Complex Modulates Chromatin Structure at Sites of Active Transcription to Fine-Tune Gene Expression. *Mol Cell* 71, 56-72 e54.

Brehm, A., Langst, G., Kehle, J., Clapier, C.R., Imhof, A., Eberharter, A., Muller, J., and Becker, P.B. (2000). dMi-2 and ISWI chromatin remodelling factors have distinct nucleosome binding and mobilization properties. *EMBO J* 19, 4332-4341.

Burgold, T., Barber, M., Kloet, S., Cramard, J., Gharbi, S., Floyd, R., Kinoshita, M., Ralser, M., Vermeulen, M., Reynolds, N.*, et al.* (2019). The Nucleosome Remodelling and Deacetylation complex suppresses transcriptional noise during lineage commitment. *EMBO J* 38.

Caussinus, E., Kanca, O., and Affolter, M. (2011). Fluorescent fusion protein knockout mediated by anti-GFP nanobody. *Nat Struct Mol Biol* 19, 117-121.

Dobin, A., Davis, C.A., Schlesinger, F., Drenkow, J., Zaleski, C., Jha, S., Batut, P., Chaisson, M., and Gingeras, T.R. (2013). STAR: ultrafast universal RNA-seq aligner. *Bioinformatics* 29, 15-21.

Eichler, K., Li, F., Litwin-Kumar, A., Park, Y., Andrade, I., Schneider-Mizell, C.M., Saumweber, T., Huser, A., Eschbach, C., Gerber, B.*, et al.* (2017). The complete connectome of a learning and memory centre in an insect brain. *Nature* 548, 175-182.

Eroglu, E., Burkard, T.R., Jiang, Y., Saini, N., Homem, C.C.F., Reichert, H., and Knoblich, J.A. (2014). SWI/SNF complex prevents lineage reversion and induces temporal patterning in neural stem cells. *Cell* 156, 1259-1273.

Estacio-Gomez, A., Hassan, A., Walmsley, E., Le, L.W., and Southall, T.D. (2020). Dynamic neurotransmitter specific transcription factor expression profiles during Drosophila development. *Biol Open* 9.

Favorov, A., Mularoni, L., Cope, L.M., Medvedeva, Y., Mironov, A.A., Makeev, V.J., and Wheelan, S.J. (2012). Exploring massive, genome scale datasets with the GenometriCorr package. *PLoS Comput Biol* 8, e1002529.

Filion, G.J., van Bemmel, J.G., Braunschweig, U., Talhout, W., Kind, J., Ward, L.D., Brugman, W., de Castro, I.J., Kerkhoven, R.M., Bussemaker, H.J.*, et al.* (2010). Systematic protein location mapping reveals five principal chromatin types in Drosophila cells. *Cell* 143, 212-224.

Forbes, S.A., Beare, D., Bindal, N., Bamford, S., Ward, S., Cole, C.G., Jia, M., Kok, C., Boutselakis, H., De, T.*, et al.* (2016). COSMIC: High-Resolution Cancer Genetics Using the Catalogue of Somatic Mutations in Cancer. *Curr Protoc Hum Genet* 91, 10 11 11-10 11 37.

Fratta, E., Coral, S., Covre, A., Parisi, G., Colizzi, F., Danielli, R., Nicolay, H.J., Sigalotti, L., and Maio, M. (2011). The biology of cancer testis antigens: putative function, regulation and therapeutic potential. *Mol Oncol* 5, 164-182.

Froldi, F., Szuperak, M., Weng, C.F., Shi, W., Papenfuss, A.T., and Cheng, L.Y. (2015). The transcription factor Nerfin-1 prevents reversion of neurons into neural stem cells. *Genes Dev* 29, 129-143.

Gomez-Del Arco, P., Perdiguero, E., Yunes-Leites, P.S., Acin-Perez, R., Zeini, M., Garcia-Gomez, A., Sreenivasan, K., Jimenez-Alcazar, M., Segales, J., Lopez-Maderuelo, D.*, et al.* (2016). The Chromatin Remodeling Complex Chd4/NuRD Controls Striated Muscle Identity and Metabolic Homeostasis. *Cell Metab* 23, 881-892.

Hassan, A., Araguas Rodriguez, P., Heidmann, S.K., Walmsley, E.L., Aughey, G.N., and Southall, T.D. (2020). Condensin I subunit Cap-G is essential for proper gene expression during the maturation of post-mitotic neurons. *Elife* 9.

Herrmann, C., Van de Sande, B., Potier, D., and Aerts, S. (2012). i-cisTarget: an integrative genomics method for the prediction of regulatory features and cis-regulatory modules. *Nucleic Acids Res* 40, e114.

Ho, J.W., Jung, Y.L., Liu, T., Alver, B.H., Lee, S., Ikegami, K., Sohn, K.A., Minoda, A., Tolstorukov, M.Y., Appert, A.*, et al.* (2014). Comparative analysis of metazoan chromatin organization. *Nature* 512, 449-452.

Hoffmann, A., and Spengler, D. (2019). Chromatin Remodeling Complex NuRD in Neurodevelopment and Neurodevelopmental Disorders. *Front Genet* 10, 682.

Hsu, T., Bagni, C., Sutherland, J.D., and Kafatos, F.C. (1996). The transcriptional factor CF2 is a mediator of EGF-R-activated dorsoventral patterning in Drosophila oogenesis. *Genes Dev* 10, 1411-1421.

Hu, Y., Comjean, A., Perrimon, N., and Mohr, S.E. (2017). The Drosophila Gene Expression Tool (DGET) for expression analyses. *BMC Bioinformatics* 18, 98.

Janic, A., Mendizabal, L., Llamazares, S., Rossell, D., and Gonzalez, C. (2010). Ectopic expression of germline genes drives malignant brain tumor growth in Drosophila. *Science* 330, 1824-1827.

Janssens, J., Aibar, S., Taskiran, II, Ismail, J.N., Gomez, A.E., Aughey, G., Spanier, K.I., De Rop, F.V., Gonzalez-Blas, C.B., Dionne, M.*, et al.* (2022). Decoding gene regulation in the fly brain. *Nature*.

Jiao, W., Spreemann, G., Ruchti, E., Banerjee, S., Shi, Y., Stowers, R.S., Hess, K., and McCabe, B.D. (2021). Intact Drosophila Whole Brain Cellular Quantitation reveals Sexual Dimorphism. *bioRxiv*, 2021.2011.2003.467146.

Krause, S.A., Overend, G., Dow, J.A.T., and Leader, D.P. (2022). FlyAtlas 2 in 2022: enhancements to the Drosophila melanogaster expression atlas. *Nucleic Acids Res* 50, D1010-D1015.

Kreher, J., Kovac, K., Bouazoune, K., Macinkovic, I., Ernst, A.L., Engelen, E., Pahl, R., Finkernagel, F., Murawska, M., Ullah, I.*, et al.* (2017). EcR recruits dMi-2 and increases efficiency of dMi-2-mediated remodelling to constrain transcription of hormone-regulated genes. *Nat Commun* 8, 14806.

Kunert, N., Wagner, E., Murawska, M., Klinker, H., Kremmer, E., and Brehm, A. (2009). dMec: a novel Mi-2 chromatin remodelling complex involved in transcriptional repression. *EMBO J* 28, 533-544.

Liao, Y., Smyth, G.K., and Shi, W. (2019). The R package Rsubread is easier, faster, cheaper and better for alignment and quantification of RNA sequencing reads. *Nucleic Acids Res* 47, e47.

Love, M.I., Huber, W., and Anders, S. (2014). Moderated estimation of fold change and dispersion for RNA-seq data with DESeq2. *Genome Biol* 15, 550.

Low, J.K., Webb, S.R., Silva, A.P., Saathoff, H., Ryan, D.P., Torrado, M., Brofelth, M., Parker, B.L., Shepherd, N.E., and Mackay, J.P. (2016). CHD4 Is a Peripheral Component of the Nucleosome Remodeling and Deacetylase Complex. *J Biol Chem* 291, 15853-15866.

Marshall, O.J., and Brand, A.H. (2015). damidseq_pipeline: an automated pipeline for processing DamID sequencing datasets. *Bioinformatics* 31, 3371-3373.

Marshall, O.J., and Brand, A.H. (2017). Chromatin state changes during neural development revealed by in vivo cell-type specific profiling. *Nat Commun* 8, 2271.

Marshall, O.J., Southall, T.D., Cheetham, S.W., and Brand, A.H. (2016). Cell-type-specific profiling of protein-DNA interactions without cell isolation using targeted DamID with next-generation sequencing. *Nat Protoc* 11, 1586-1598.

Nichols, C.D., Becnel, J., and Pandey, U.B. (2012). Methods to assay Drosophila behavior. *J Vis Exp*.

Nitarska, J., Smith, J.G., Sherlock, W.T., Hillege, M.M., Nott, A., Barshop, W.D., Vashisht, A.A., Wohlschlegel, J.A., Mitter, R., and Riccio, A. (2016). A Functional Switch of NuRD Chromatin Remodeling Complex Subunits Regulates Mouse Cortical Development. *Cell Rep* 17, 1683-1698.

O'Shaughnessy-Kirwan, A., Signolet, J., Costello, I., Gharbi, S., and Hendrich, B. (2015). Constraint of gene expression by the chromatin remodelling protein CHD4 facilitates lineage specification. *Development* 142, 2586-2597.

Preissl, S., Fang, R., Huang, H., Zhao, Y., Raviram, R., Gorkin, D.U., Zhang, Y., Sos, B.C., Afzal, V., Dickel, D.E.*, et al.* (2018). Single-nucleus analysis of accessible chromatin in developing mouse forebrain reveals cell-type-specific transcriptional regulation. *Nat Neurosci* 21, 432-439.

Quinlan, A.R., and Hall, I.M. (2010). BEDTools: a flexible suite of utilities for comparing genomic features. *Bioinformatics* 26, 841-842.

Ragheb, R., Gharbi, S., Cramard, J., Ogundele, O., Kloet, S.L., Burgold, T., Vermeulen, M., Reynolds, N., and Hendrich, B. (2020). Differential regulation of lineage commitment in human and mouse primed pluripotent stem cells by the nucleosome remodelling and deacetylation complex. *Stem Cell Res* 46, 101867.

Rais, Y., Zviran, A., Geula, S., Gafni, O., Chomsky, E., Viukov, S., Mansour, A.A., Caspi, I., Krupalnik, V., Zerbib, M.*, et al.* (2013). Deterministic direct reprogramming of somatic cells to pluripotency. *Nature* 502, 65-70.

Ravenscroft, T.A., Janssens, J., Lee, P.T., Tepe, B., Marcogliese, P.C., Makhzami, S., Holmes, T.C., Aerts, S., and Bellen, H.J. (2020). Drosophila Voltage-Gated Sodium Channels Are Only Expressed in Active Neurons and Are Localized to Distal Axonal Initial Segment-like Domains. *J Neurosci* 40, 7999-8024.

Reddington, J.P., Garfield, D.A., Sigalova, O.M., Karabacak Calviello, A., Marco-Ferreres, R., Girardot, C., Viales, R.R., Degner, J.F., Ohler, U., and Furlong, E.E.M. (2020). Lineage-Resolved Enhancer and Promoter Usage during a Time Course of Embryogenesis. *Dev Cell* 55, 648-664 e649.

Reddy, B.A., Bajpe, P.K., Bassett, A., Moshkin, Y.M., Kozhevnikova, E., Bezstarosti, K., Demmers, J.A., Travers, A.A., and Verrijzer, C.P. (2010). Drosophila transcription factor Tramtrack69 binds MEP1 to recruit the chromatin remodeler NuRD. *Mol Cell Biol* 30, 5234-5244.

Rhee, D.Y., Cho, D.Y., Zhai, B., Slattery, M., Ma, L., Mintseris, J., Wong, C.Y., White, K.P., Celniker, S.E., Przytycka, T.M.*, et al.* (2014). Transcription factor networks in Drosophila melanogaster. *Cell Rep* 8, 2031-2043.

Southall, T.D., Davidson, C.M., Miller, C., Carr, A., and Brand, A.H. (2014). Dedifferentiation of neurons precedes tumor formation in Lola mutants. *Dev Cell* 28, 685-696.

Southall, T.D., Gold, K.S., Egger, B., Davidson, C.M., Caygill, E.E., Marshall, O.J., and Brand, A.H. (2013). Cell-type-specific profiling of gene expression and chromatin binding without cell isolation: assaying RNA Pol II occupancy in neural stem cells. *Dev Cell* 26, 101-112.

Tie, F., Furuyama, T., Prasad-Sinha, J., Jane, E., and Harte, P.J. (2001). The Drosophila Polycomb Group proteins ESC and E(Z) are present in a complex containing the histone-binding protein p55 and the histone deacetylase RPD3. *Development* 128, 275-286.

Tong, J.K., Hassig, C.A., Schnitzler, G.R., Kingston, R.E., and Schreiber, S.L. (1998). Chromatin deacetylation by an ATP-dependent nucleosome remodelling complex. *Nature* 395, 917-921.

Unhavaithaya, Y., Shin, T.H., Miliaras, N., Lee, J., Oyama, T., and Mello, C.C. (2002). MEP-1 and a homolog of the NURD complex component Mi-2 act together to maintain germline-soma distinctions in C. elegans. *Cell* 111, 991-1002.

Wade, P.A., Jones, P.L., Vermaak, D., and Wolffe, A.P. (1998). A multiple subunit Mi-2 histone deacetylase from Xenopus laevis cofractionates with an associated Snf2 superfamily ATPase. *Curr Biol* 8, 843-846.

Wang, H.B., and Zhang, Y. (2001). Mi2, an auto-antigen for dermatomyositis, is an ATP-dependent nucleosome remodeling factor. *Nucleic Acids Res* 29, 2517-2521.

Wang, Z., Zang, C., Cui, K., Schones, D.E., Barski, A., Peng, W., and Zhao, K. (2009). Genome-wide mapping of HATs and HDACs reveals distinct functions in active and inactive genes. *Cell* 138, 1019-1031.

Xue, Y., Wong, J., Moreno, G.T., Young, M.K., Cote, J., and Wang, W. (1998). NURD, a novel complex with both ATP-dependent chromatin-remodeling and histone deacetylase activities. *Mol Cell* 2, 851-861.

Yamada, T., Yang, Y., Hemberg, M., Yoshida, T., Cho, H.Y., Murphy, J.P., Fioravante, D., Regehr, W.G., Gygi, S.P., Georgopoulos, K.*, et al.* (2014). Promoter decommissioning by the NuRD chromatin remodeling complex triggers synaptic connectivity in the mammalian brain. *Neuron* 83, 122-134.

Yoshida, T., Hazan, I., Zhang, J., Ng, S.Y., Naito, T., Snippert, H.J., Heller, E.J., Qi, X., Lawton, L.N., Williams, C.J.*, et al.* (2008). The role of the chromatin remodeler Mi-2beta in hematopoietic stem cell self-renewal and multilineage differentiation. *Genes Dev* 22, 1174-1189.

Zacharioudaki, E., Falo Sanjuan, J., and Bray, S. (2019). Mi-2/NuRD complex protects stem cell progeny from mitogenic Notch signaling. *Elife* 8.

Zhang, W., Aubert, A., Gomez de Segura, J.M., Karuppasamy, M., Basu, S., Murthy, A.S., Diamante, A., Drury, T.A., Balmer, J., Cramard, J.*, et al.* (2016). The Nucleosome Remodeling and Deacetylase Complex NuRD Is Built from Preformed Catalytically Active Sub-modules. *J Mol Biol* 428, 2931-2942.

Zhang, Y., LeRoy, G., Seelig, H.P., Lane, W.S., and Reinberg, D. (1998). The dermatomyositis-specific autoantigen Mi2 is a component of a complex containing histone deacetylase and nucleosome remodeling activities. *Cell* 95, 279-289.

Ziffra, R.S., Kim, C.N., Ross, J.M., Wilfert, A., Turner, T.N., Haeussler, M., Casella, A.M., Przytycki, P.F., Keough, K.C., Shin, D.*, et al.* (2021). Single-cell epigenomics reveals mechanisms of human cortical development. *Nature* 598, 205-213.